


## Article

# The Protection of Building Materials of Historical Monuments with Nanoparticle Suspensions

Efstathia I. Pavlakou <sup>1,2</sup>, Anastasios G. Agrafiotis <sup>1</sup>, Theokleiti G. Tsolaki <sup>1</sup>, Christine Lemonia <sup>1</sup>, Emily Zouvani <sup>1</sup>, Christakis A. Paraskeva <sup>1,2</sup>  and Petros G. Koutsoukos <sup>2,3,\*</sup>

- <sup>1</sup> Laboratory of Transport Phenomena and Physicochemical Hydrodynamics, Department of Chemical Engineering, University of Patras, 26500 Patras, Greece; pavlakou@chemeng.upatras.gr (E.I.P.); cmng3373@upnet.upatras.gr (A.G.A.); cmng3536@upnet.upatras.gr (T.G.T.); up1055885@upnet.upatras.gr (C.L.); up1049832@upnet.upatras.gr (E.Z.); takisp@chemeng.upatras.gr (C.A.P.)
- <sup>2</sup> FORTH/ICE-HT, Institute of Chemical Engineering Sciences, 26500 Patras, Greece
- <sup>3</sup> Laboratory of Inorganic and Analytic Chemistry, Department of Chemical Engineering, University of Patras, 26500 Patras, Greece
- \* Correspondence: pgk@chemeng.upatras.gr



**Citation:** Pavlakou, E.I.; Agrafiotis, A.G.; Tsolaki, T.G.; Lemonia, C.; Zouvani, E.; Paraskeva, C.A.; Koutsoukos, P.G. The Protection of Building Materials of Historical Monuments with Nanoparticle Suspensions. *Heritage* **2021**, *4*, 3970–3986. <https://doi.org/10.3390/heritage4040218>

Academic Editors: Elisabetta Zendri, Ekaterini Delegou, Michael Turner, Antonia Moropoulou and Rodica Mariana Ion

Received: 8 September 2021

Accepted: 25 October 2021

Published: 27 October 2021

**Publisher's Note:** MDPI stays neutral with regard to jurisdictional claims in published maps and institutional affiliations.



**Copyright:** © 2021 by the authors. Licensee MDPI, Basel, Switzerland. This article is an open access article distributed under the terms and conditions of the Creative Commons Attribution (CC BY) license (<https://creativecommons.org/licenses/by/4.0/>).

**Abstract:** Marble and limestone have been extensively used as building materials in historical monuments. Environmental, physical, chemical and biological factors contribute to stone deterioration. The rehabilitation of stone damage and the delay of further deterioration is of utmost importance. Inorganic nanoparticles having chemical and crystallographic affinity with building materials is very important for the formation of protective coatings or overlayers. In the present work, we have tested the possibility of treating calcitic materials with suspensions of amorphous calcium carbonate (am-CaCO<sub>3</sub>, ACC) and amorphous silica (AmSiO<sub>2</sub>). Pentelic marble (PM) was selected as the test material to validate the efficiency of the nanoparticle suspension treatment towards dissolution in undersaturated solutions and slightly acidic pH (6.50). Suspensions of ACC and AmSiO<sub>2</sub> nanoparticles were prepared by spontaneous precipitation from supersaturated solutions and by tetraethyl orthosilicate (TEOS) hydrolysis, respectively. The suspensions were quite stable (nine days for ACC and months for AmSiO<sub>2</sub>). ACC and AmSiO<sub>2</sub> particles were deposited on the surface of powdered PM. The rates of dissolution of PM were measured in solutions undersaturated with respect to calcite at a constant pH of 6.50. For specimens treated with ACC and AmSiO<sub>2</sub> suspensions, the measured dissolution rates were significantly lower. The extent of the rate of dissolution reduction was higher for AmSiO<sub>2</sub> particles on PM. Moreover, application of the nanoparticles on the substrate during their precipitation was most efficient method.

**Keywords:** amorphous calcium carbonate (ACC); amorphous silica; synthesis; characterization; coatings; dissolution rates

## 1. Introduction

Marble and limestone are commonly used building materials for historical monuments, especially in the countries in the Mediterranean basin. These building materials contain mainly calcite, which makes them susceptible to chemical deterioration from wet precipitation. This problem is intensified at conditions of environmental pollution in which the concentration of acid gases (SO<sub>2</sub>, NO<sub>x</sub>) is sufficiently high to render rainwater acidic [1]. The presence of microorganisms on the surface of monuments contributes to stone deterioration over time due to changes in the chemical microenvironment and coloration as well as mechanical damage. Human interventions aimed at the restoration of monuments may also lead to further destruction because of the use of improper materials or because of material mismatch [2,3]. The importance of cultural heritage calls for the development of new materials, especially for materials which can effectively repair building materials

and artefacts and treat natural stone. Nanotechnology is a very important resource for these materials [4]. New materials for the remediation of damaged stones should exhibit structural affinity for the substrates. Colloid and material science have contributed significantly to art (paper, canvas, and wood) preservation over time through the use of nanostructured fluids (microemulsions and micellar solutions), chemical gels and alkaline nonaqueous nanoparticles dispersions [2]. Several attempts for the consolidation and protection of stones of historic monuments have involved the use of polymeric compounds (acrylates, alkoxysilanes). Fluorinated polymers and hybrid organic–inorganic coatings are the most promising materials in the field of monument protection [3]. Alkoxysilanes and modified silica nanoparticles are applied on stone artifacts (sandstone, marble and granite) as protective water repellent coatings [5]. Materials consisting of an ethyl silicate matrix with colloidal  $\text{TiO}_2$  and  $\text{SiO}_2$  nanoparticles were shown to be effective in stabilizing porous limestone [6]. The hybrid material consisting of  $\text{SiO}_2$  and  $\text{TiO}_2$  showed encouraging results in the protection and self-cleaning of marble [7,8]. Enhancement of hydrophobicity of stone-based monuments was reported for polymer–silica nanoparticle composite films on mineral substrates (natural marble and home made calcium carbonate blocks) [9]. Clay,  $\text{SiO}_2$ ,  $\text{Ca(OH)}_2$  and  $\text{CaCO}_3$  were satisfactory for the consolidation of limestone [10]. Calcium carbonate–polymer nanocomposite increased the impermeability of limestone and improve its mechanical properties [11]. Composites of amorphous calcium carbonate (ACC) and amorphous calcium oxalate (ACO) with alkoxysilane gels applied for the protection of monument building materials without silicates (marble, calcarenite, gypsum) resulted in the increase of surface hydrophobicity and improved resistance to acid attack [12]. Siloxane coatings with  $\text{SiO}_2$ ,  $\text{Al}_2\text{O}_3$ ,  $\text{SnO}_2$  and  $\text{TiO}_2$  nanoparticles yielded superhydrophobic surfaces [13]. Barium, calcium and strontium hydroxide nanoparticles have also been used successfully for the restoration of wall paintings and in trials on sandstone and marble [14–17]. During consolidation by  $\text{Ca(OH)}_2$  particles upon exposure to atmospheric  $\text{CO}_2$ , ACC formation takes place, which is subsequently converted to the thermodynamically more stable calcite [18]. Besides their crystallographic characteristics, these two calcium carbonates differ significantly in particle size (almost 1:10). The very small size of ACC particles is expected to favor penetration into the meso- and macropores of damaged stone. Amorphous silica particles suspended in water, used for the treatment of stone, penetrated inside stone matrix to a very shallow depth which increased upon suspending the particles in alcohol [19].

In the present work,  $\text{CaCO}_3$  and silica  $\text{SiO}_2$  nanoparticle suspensions were prepared from highly supersaturated solutions and from the hydrolysis of tetraortho silicate ( $\text{Si(OC}_2\text{H}_5)_4$ , TEOS) in ethanolic solutions, respectively. Both solid particles in the respective suspensions have high crystallographic affinity for calcite. The solid particles in the suspensions were characterized by physicochemical methods (powder X-ray diffraction, XRD; measurements of their specific surface area with nitrogen adsorption according to the Brunnauer–Emmet–Teller method, BET; Fourier transformed infra-red spectroscopy, FTIR; micro-Raman, mR; and thermogravimetric analysis, TGA). The stability of the nanoparticle suspensions was assessed from the mean particle size measured with laser diffraction. The effect of the presence of the cationic surfactant hexadecyltrimethylammonium bromide (CTAB) on the stability of the nanoparticle suspensions was investigated. The stability of the unstable ACC and of the respective suspensions was investigated in isopropyl alcohol. The deposition of the ACC and  $\text{SiO}_2$  nanoparticles in their suspensions was carried out on powdered Pentelic marble, to maximize the surface area. Slabs of PM were ground in a ball mill to a powder with a grain size of between 600–1700  $\mu\text{m}$ . The results of the treated materials with the particles were evaluated by dissolution experiments in which the rates of dissolution of the specimens were measured in undersaturated solutions of calcium carbonate (pH 6.50, 25.0  $^\circ\text{C}$ ). Earlier work has shown that accelerated dissolution tests of powdered building materials yielded comparable results with respective dissolution experiments in which intact stone slabs were used [20]. The present work may be considered preliminary, proof-of-concept work, for the evaluation of new materials. Although

ACC has been identified in conservation processes, especially with nanolime, up to the present to our knowledge, it has not been used in the form of stable suspensions, as a primary stone conservation material. Provided that the results are encouraging in the sense that they show protection of treated stone material, the work may be expanded to a second stage in order to involve blocks or test specimens of stone material, either intact or artificially deteriorated. The results in the present work are only preliminary, pointing to potential applications, and they allow for more detailed insight on the interactions of ACC and AmSiO<sub>2</sub> particles with marble. The further task of this work is the preparation of the composite material ACC–AmSiO<sub>2</sub>, which we anticipate will be able to provide both consolidation and resistance to chemical dissolution of treated stone.

## 2. Experimental

ACC and SiO<sub>2</sub> were prepared as suspensions. CaCO<sub>3</sub> particles were prepared by precipitation from supersaturated solutions, the composition of which is summarized in Table 1.

**Table 1.** Experimental conditions for the synthesis of ACC suspensions. 25 °C; Total duration of precipitation before the separation of the solids from mother liquor: 150 s.

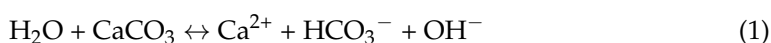
Parameter/Preparation	1	2	3	4	5
Concentration of DMC (M)	0.1	0.1	0.1	0.1	0.05
Concentration of CaCl <sub>2</sub> ·2H <sub>2</sub> O (M)	0.05	0.05	0.05	0.05	0.01
Concentration of NaOH (M)	0.3	0.3	0.3	0.3	0.1
Concentration of CTAB (ppm)	-	1	10	100	-

The composition of the solutions was selected so that the solution supersaturation with respect to calcium carbonate was very high, and the solid phase anticipated to form was ACC [21,22]. Preparations 1–4 (Table 1), were done both in the absence and in the presence of cetrimonium bromide ([C<sub>16</sub>H<sub>33</sub>N(CH<sub>3</sub>)<sub>3</sub>]Br; cetyltrimethylammonium bromide; and hexadecyltrimethylammonium bromide; CTAB) at concentrations of 1, 10 and 100 ppm. Specifically, two solutions were mixed in a batch reactor at 25 °C. The first solution was dimethyl carbonate (DMC) and sodium chloride (NaCl) and the second solution was calcium chloride (CaCl<sub>2</sub>). The two solutions upon mixing were stirred vigorously with a PTFE coated bar and a magnetic stirrer for 2.5 min. The suspension of calcium carbonate solid particles was filtered under vacuum with membrane filters (cellulose nitrate 0.2 µm), and the solid on the filters was rinsed with acetone and freeze dried. The solid, was identified by XRD and the morphology and particle size distribution was assessed from pictures obtained with scanning electron microscopy, SEM. The solid phase was further characterized with Fourier Transformed InfraRed Spectroscopy (FTIR), micro Raman spectroscopy (mR) and Thermo-Gravimetric Analysis (TGA). The respective specific surface area was measured by the Brunnauer, Emmet, Teller (BET) nitrogen absorption method. Extended absorption isotherm measurements were used for the calculation of porosity. In the case of powdered PM, dried material was used. For the PM samples treated with the suspensions, the samples were separated from the suspensions by filtration, washed with triply distilled water and dried overnight at 60 °C. Silicon oxide nanoparticles were prepared by hydrolysis of TEOS [23]. Ethanol (C<sub>2</sub>H<sub>5</sub>OH, 95% in water) and ammonia (NH<sub>3</sub>, 32%) solutions were added in a batch reactor and were stirred with a magnetic stirrer for 30 min. Next, the appropriate amount of TEOS was added and stirring was continued for an additional hour. In the silica precipitation in the presence of CTAB, the latter was added in an ethanol–ammonia solution. The solid formed by hydrolysis was characterized by XRD and the morphology was investigated by SEM. The stability of the silica suspensions in the absence and in the presence of CTAB was monitored as a function of time from measurements of the particle size distribution (PSD) in the suspensions. The silica particles that were formed were treated in an ultrasonic bath for 1, 2, 5 and 7 min. The suspended

particles were separated from the suspensions, filtered through membrane filters (0.1  $\mu\text{m}$ ) and analyzed by thermogravimetric analysis (TGA).

Powdered Pentelic marble (PM) was used as a model system for  $\text{CaCO}_3$  and  $\text{SiO}_2$  nanoparticle deposition, to test the effect of application of the suspensions of particles prepared on its protection from dissolution in acidic undersaturated solutions. PM from slabs was ground in a ball mill, until a powder of particles with sizes (equivalent sphere diameter) between 500–1500  $\mu\text{m}$  was obtained. Each of these particles contained a large number marble grains consisting of calcite crystals, separated in their boundaries, consisting of silica minerals. These granulated PM particles provide a reasonable representation of flat marble surfaces from the point of view of chemical and mineralogical composition, while exhibiting on the other hand a sufficiently large surface area to observe and monitor surface-controlled processes such as dissolution in undersaturated solutions. Two methods for the deposition of ACC nanoparticles on PM were applied: According to the first method (method CCA), the powdered PM was suspended in the DMC and  $\text{CaCl}_2$  solution mixture. The suspension of PM powder was thoroughly mixed until it was homogeneous, and next, the appropriate sodium hydroxide solution was added to make the suspension alkaline (pH Ca.10) and thus initiate hydrolysis of DMC, which resulted in the precipitation of ACC. In the second method (method CCB), the powdered PM was introduced in the solutions mixture immediately past the onset of formation of ACC. From the practical point of view, both methods represented situations in which a suspension of ACC was deposited on the surface of PM, but they differed in the timing of deposition: in CCA, deposits were formed in situ during precipitation on the substrate, and in CCB, a suspension of ACC particles interacted with the substrate. Amorphous  $\text{SiO}_2$  particles ( $\text{AmSiO}_2$ ) were prepared by hydrolysis of TEOS (0.29 M) in ammonia solution, (0.67 M) in 95% ethanol solutions at 25  $^\circ\text{C}$ . The duration of the hydrolysis process was 180 min.  $\text{AmSiO}_2$  suspensions were also prepared at the same conditions, in the presence of 1, 5 and 10 ppm of CTAB in the hydrolysis medium. The deposition of amorphous  $\text{SiO}_2$  nanoparticles was also done with two methods:  $\text{AmSiA}$ , in which powdered PM was suspended in the ethanol–ammonia mixture followed by the introduction and subsequent hydrolysis of TEOS, and  $\text{AmSiB}$ , in which the powdered PM was added after the initiation of the rapid hydrolysis of TEOS. The solids at the end of the synthesis were separated from the liquid by filtration and were characterized by XRD and measurements of their specific surface area (BET). The morphology of the preparations was studied by SEM.

The PM dissolution (treated and untreated) was studied in solutions undersaturated with respect to calcium carbonate. Undersaturated solutions were prepared directly in a batch reactor thermostatic at  $25.0 \pm 0.1$   $^\circ\text{C}$  with circulating water. The solutions were prepared by mixing  $\text{CaCl}_2 \cdot 2\text{H}_2\text{O}$  and  $\text{NaHCO}_3$  solutions (final solutions concentrations 1.25 mM) and pH was adjusted to 6.50. The ionic strength of the solutions was adjusted to 0.15 M with the addition of stock NaCl solution as needed. Following pH adjustment by the addition of standard hydrochloric acid solution, accurately weighted test solid was introduced into the undersaturated solutions. The solutions' pH increased as a result of the dissolution of calcium carbonate:



Changes in the solution pH as small as 0.01 pH units triggered the addition of standard HCl solution (0.01 M) from the precision syringe of a computer-controlled pH stat system. The dissolution process was thus measured at a constant pH until the solution undersaturation decreased sufficiently to stop additions, due to the pH reaching a point where it was practically unchanged. Samples were withdrawn and filtered through membrane filters. The filtrates were analyzed for total calcium by atomic absorption spectrometry (AAS, Perkin Elmer AAnalyst 300) and for dissolved silicates spectrophotometrically (Perkin Elmer lambda 35) as needed. The experimental set-up for the dissolution tests is shown in Figure 1.

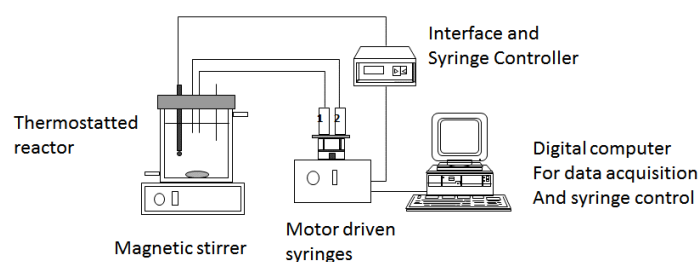


**Figure 1.** Experimental set-up for the measurement of dissolution of calcitic materials at constant pH.

### 3. Results and Discussion

#### 3.1. $\text{CaCO}_3$ Particles/Suspensions

Calcium carbonate, in preparations 1–4 of Table 1 (in the absence and in the presence of CTAB) yielded calcite and vaterite and small amounts of ACC. The presence of ACC was a clear indication of the formation of ACC and its subsequent transformation to vaterite, and to the most stable calcite. In the absence of CTAB, the crystalline phases identified in the precipitate were vaterite and portlandite (Figure 2a). At all test conditions, calcium hydroxide (portlandite) precipitated as well from the supersaturated solutions because of the high initial pH of the solutions ( $>10$ ), as may be seen in the XRD profiles shown in Figure 2b. It is interesting to note that portlandite was stable for a long time, although it is reported that the carbonation reaction of calcium carbonate is quite fast [18,23]. Perhaps the stabilization towards carbonization is due to the substrate or to the presence of the other mineral phases. Specifically, in the absence and in the presence of low CTAB (1 ppm) concentrations, vaterite precipitated together with ACC, showing that the presence of the cationic surfactant slowed to some extent the conversion of ACC to vaterite. At higher concentrations of the test cationic surfactant (10, 100 ppm) calcite was also found, clearly coming from the conversion of the less stable vaterite.

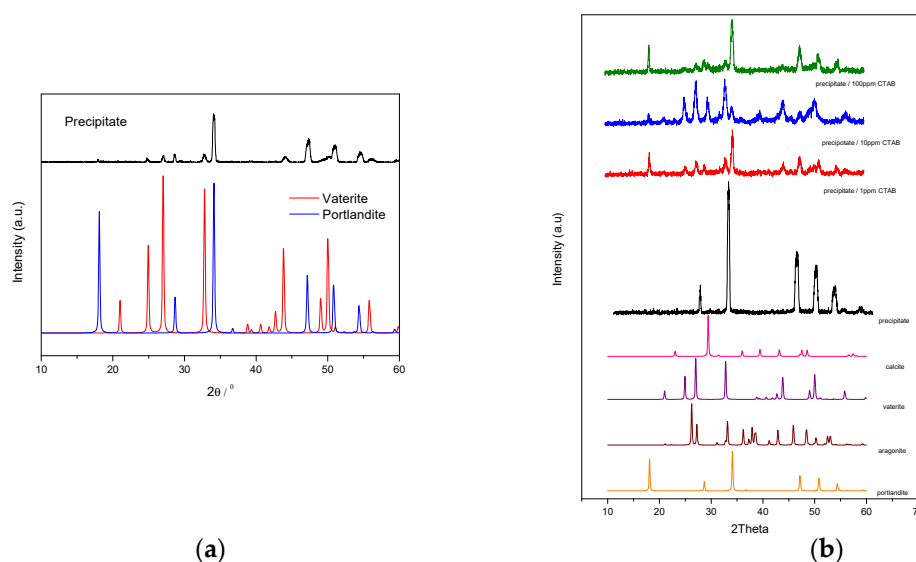


**Figure 2.** Powder X-ray diffraction pattern of  $\text{CaCO}_3$  precipitates in the absence (a) and in the presence of CTAB (b).

In the SEM photographs (Figure 3), vaterite particles may be seen (mean diameter 1.0–1.5  $\mu\text{m}$ ) both in the absence and in the presence of CTAB. The very small vaterite particle size showed that this phase was formed by conversion of the initially formed ACC. In the presence of the cationic surfactant other than vaterite, ACC nanoparticles were also to a significant extent converting to vaterite (Figure 3b–d). In Figure 3a, as may be seen, the precipitate consists of ca. 100 nm ACC particles agglomerated to vaterite converting to calcite (developing crystal faces typical of calcite).



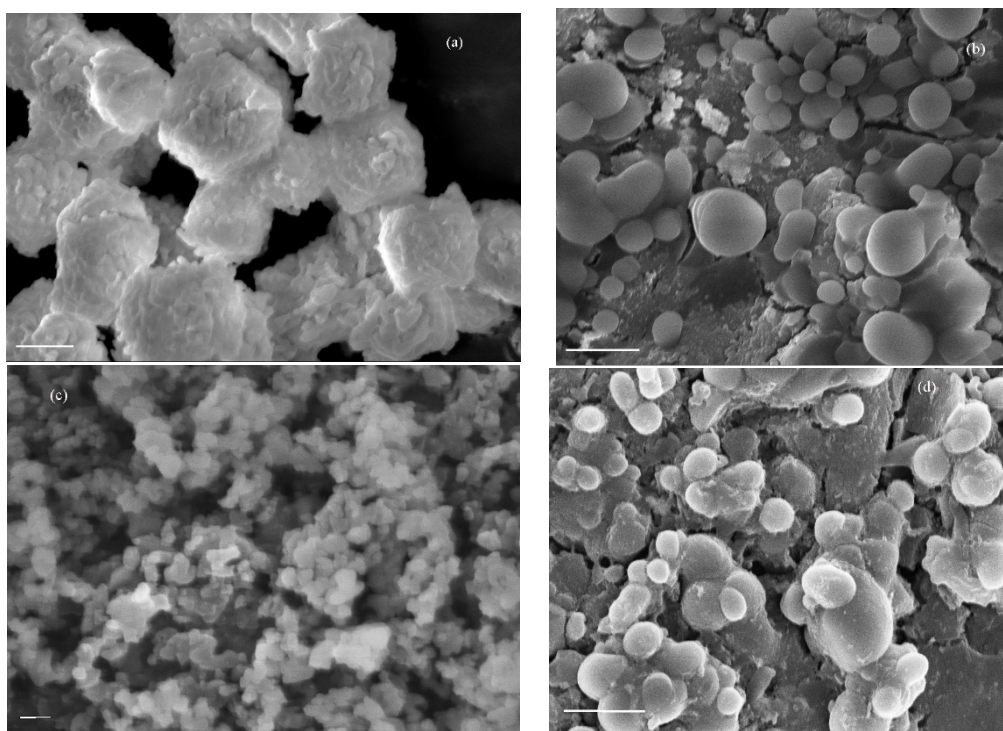


**Figure 3.**  $\text{CaCO}_3$  particles precipitated according to conditions summarized in Table 1: (a) in the absence of CTAB, Bar 1  $\mu\text{m}$ ; (b) 1 ppm CTAB, Bar 2  $\mu\text{m}$ ; (c) 10 ppm, Bar 200 nm; (d) 100 ppm CTAB, Bar 2  $\mu\text{m}$ .

The IR spectra of the precipitates are shown in Figure 4. The characteristic band at  $745\text{ cm}^{-1}$ , corresponding to vaterite, was present in all precipitates [24]. The band at  $1074\text{ cm}^{-1}$  of the solid precipitated in the presence of CTAB corresponds to ACC [25]. In the absence of the cationic surfactant, the band of the precipitated solid at  $848\text{ cm}^{-1}$  corresponded to calcite. The strong band at  $713\text{ cm}^{-1}$ , corresponding to calcite [24], was found in all precipitated solids. The absorption bands at  $1087\text{ cm}^{-1}$  suggested the presence of ACC, in the form of precursor to calcite and vaterite polymorphic phases [25]. The broad band at  $2700\text{--}3600\text{ cm}^{-1}$  is suggested to correspond to the water content of ACC. The bands at  $2352$  and  $3642\text{ cm}^{-1}$  suggested the presence of portlandite [26–30].

The Raman spectra, shown in Figure 5, revealed the characteristic peaks of calcite and vaterite. The peak at  $1085\text{ cm}^{-1}$  is characteristic for ACC, corresponding to the  $\nu_1$  vibration [25]. Calcite was identified in the precipitates formed in the presence of higher CTAB concentrations (10, 100 ppm) from the peaks at  $155\text{ cm}^{-1}$ ,  $282\text{ cm}^{-1}$ , and  $711\text{ cm}^{-1}$ , which belong to lattice modes. The doublets of the vibration modes  $1075\text{--}1090\text{ cm}^{-1}$  ( $\nu_1$ ; all precipitates except of the precipitate formed in the presence of 10 ppm CTAB) and  $740\text{--}750\text{ cm}^{-1}$  ( $\nu_4$ ) confirmed the presence of vaterite. Strong peaks at  $105$ ,  $114$ ,  $267$ ,  $300\text{ cm}^{-1}$  correspond, also, to vaterite (formed both in the absence and in the presence of 1 ppm CTAB). The presence of aragonite was identified at  $206\text{ cm}^{-1}$ , both in the absence and in the presence of 1 ppm CTAB and in higher concentrations (10, 100 ppm) at  $155\text{ cm}^{-1}$  [31,32]. Finally, portlandite was identified in all preparations at  $350\text{ cm}^{-1}$ , while absence of CTAB showed an extra band at  $350\text{ cm}^{-1}$  [33]. Thermogravimetric analysis results of the precipitates are shown in Figure 6. The first weight reduction ( $85\text{--}110^\circ\text{C}$ ) is due to the removal of naturally absorbed water. At the temperature range of  $400\text{--}450^\circ\text{C}$ , the weight difference is due to the combustion of the organic part of the precipitate, resulting from the hydrolysis of DMC during the synthesis of  $\text{CaCO}_3$ . The final weight loss was observed at  $650\text{--}700^\circ\text{C}$  and was due to the removal of carbon dioxide during the conversion of calcium carbonate to calcium oxide at this temperature range.

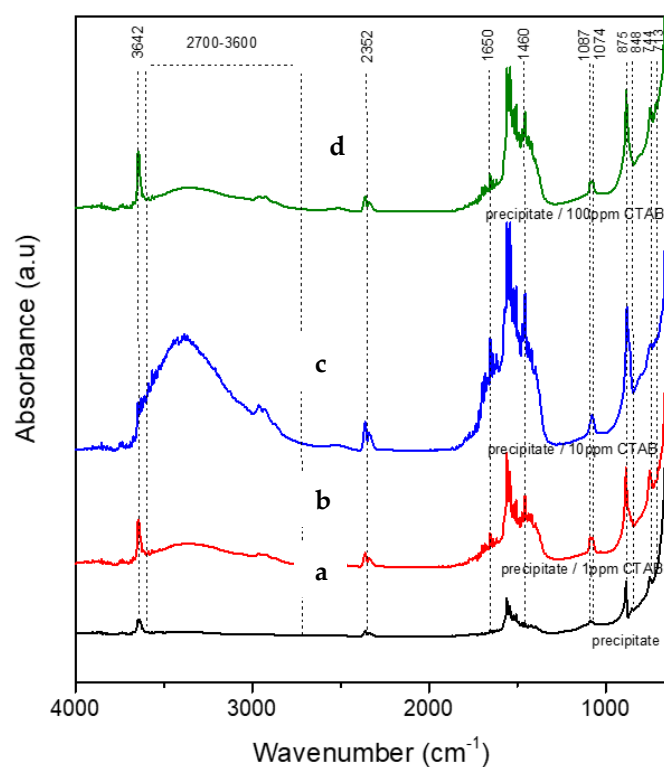


**Figure 4.** FTIR spectra of the precipitate formed: (a) in the absence of CTAB; and in the presence of (b) 1 ppm CTAB; (c) 10 ppm CTAB; (d) 100 ppm CTAB.

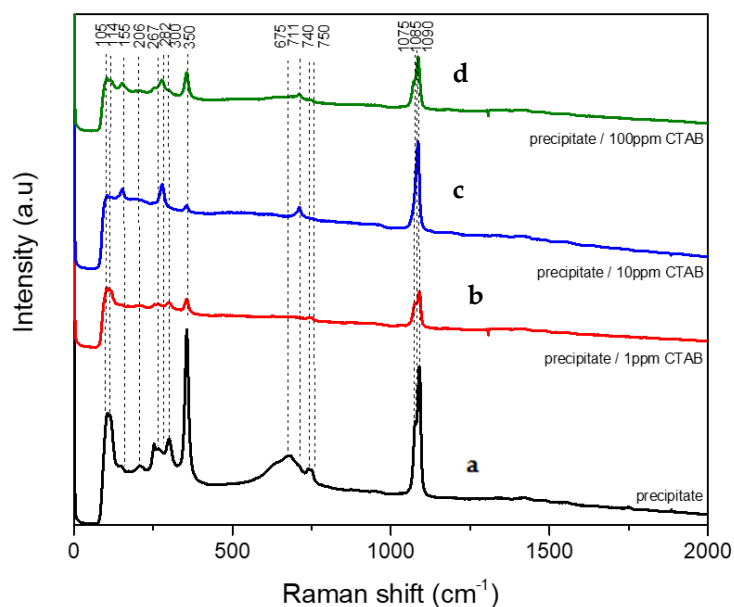


**Figure 5.** Micro-Raman spectra of  $\text{CaCO}_3$  precipitates formed: (a) in the absence of CTAB; and in the presence of (b) 1 ppm CTAB; (c) 10 ppm CTAB; (d) 100 ppm CTAB.

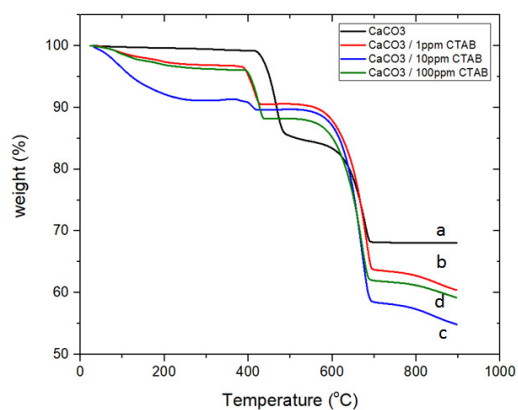


**Figure 6.** TGA analysis profiles of  $\text{CaCO}_3$  precipitates: (a) in the absence of CTAB (black line); and in the presence of (b) 1 ppm CTAB; (c) 10 ppm; (d) 100 ppm CTAB.

The formation of ACC nanoparticles by precipitation in the conditions used for preparation 5 (Table 1), was confirmed by the XRD profile shown in Figure 7a. As may be seen both from the lack of sharp reflections and from the low counts number, the respective solids were predominantly amorphous. The morphology of the precipitated solid, as may be seen from SEM photographs, showed the formation of spherical particles, with sizes of about 300 nm (Figure 7b). The BET specific surface area of the precipitate was measured and was found to be equal to  $4.7 \text{ m}^2 \cdot \text{g}^{-1}$ .

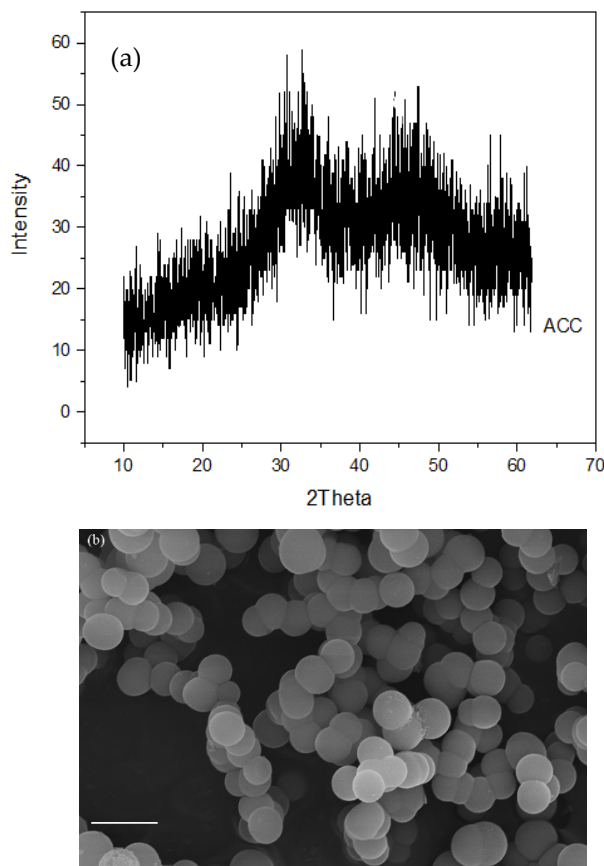


**Figure 7.** (a) Powder X-ray diffraction pattern; (b) SEM photographs of ACC particles formed at the conditions of preparation 5 (Table 1); Bar 1  $\mu\text{m}$ .

An important property of nanomaterials is their high specific surface area in comparison with the respective area of the macroscopic material. Their application therefore



implies a drastically larger interaction surface with the environment. The application of suspended nanoparticles on stone, from a practical point of view, is often done by brushes or by spray applications. In the present work, the application of suspended particles was done by suspending the powdered PM, which presents the advantage of increasing the surface area of interaction, while on the other hand, the advantage of simulation of the macroscopic size of treated stone is preserved. Each of the grains of the PM powder consists of particles which make up a miniature of the stone surface. Undoubtedly, further development is needed before going on to conservation practice, to ensure effective penetration of the suspension to the deteriorated parts of the stone. The main task of the present work was to prove a significant increase in the resistance of the treated stone material to dissolution caused by wet precipitation. ACC suspended in water is shown to transform in rather short times in aqueous media [18]. To extend further the stability of the suspended solid phase, ACC particles, after their separation from the mother liquor by freeze drying, were suspended in isopropyl alcohol. The stability of the suspensions was monitored for two weeks; the morphology and particle size were checked from a number of SEM photographs, as may be seen in Figure 8; their suspension into the solvent resulted in their stability in the form of ACC with sizes lower than 500 nm for nine days. Their transformation into calcite took place during the following days. Specifically, over the first nine days (Figure 8a–d), the spherical nanoparticles were seen exclusively without significant changes in size. Past this time, the morphology of the particles started to change, showing conversion to rhombohedral calcite, although the size changes were not significant.

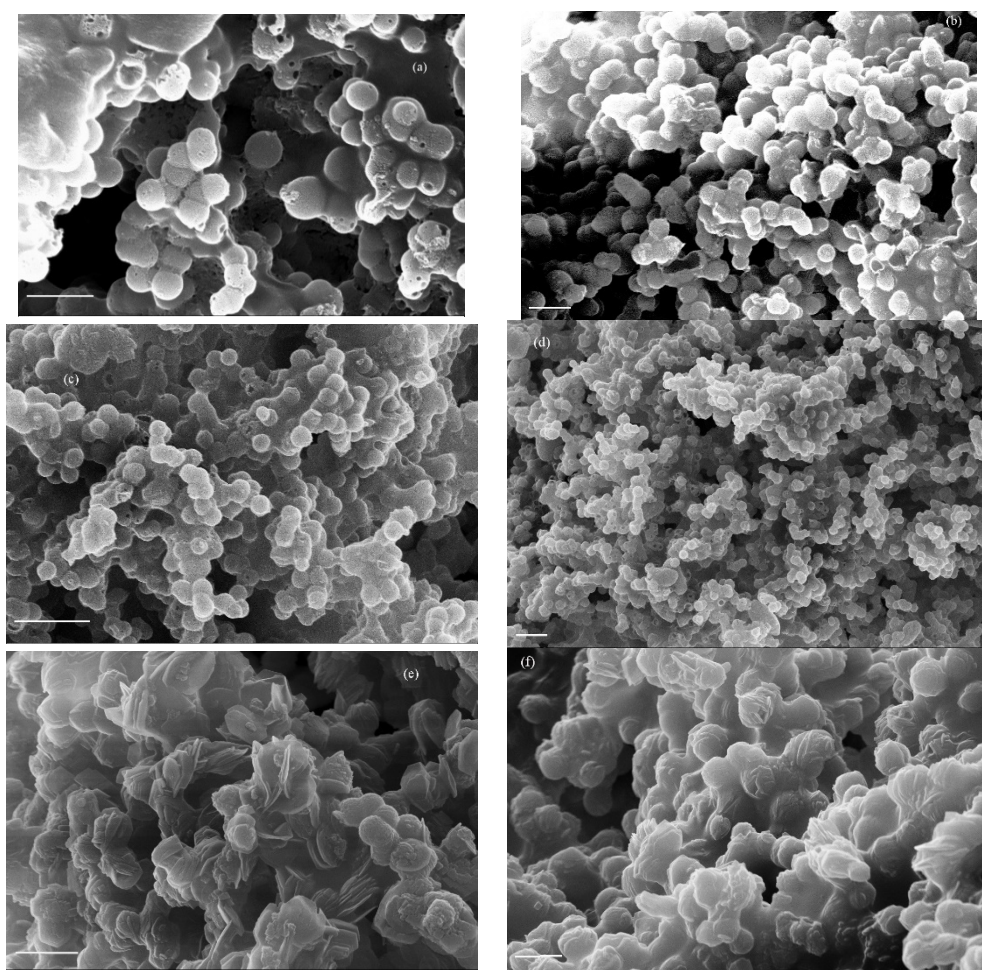


**Figure 8.** CaCO<sub>3</sub> suspensions in isopropyl alcohol. Evolution of crystal shape and size past: (a) 1 day (bar 1  $\mu$ m), (b) 6 days (bar 1  $\mu$ m), (c) 8 days (bar 2  $\mu$ m), (d) 9 days (bar 2  $\mu$ m), (e) 13 days (bar 1  $\mu$ m), (f) 14 days (bar 1  $\mu$ m).

From the results shown so far, it may be concluded that the formation of ACC is feasible and that stable suspensions can be prepared in isopropyl alcohol. It should be noted that the dry ACC powder, preserved at  $-24\text{ }^{\circ}\text{C}$ , did not show any changes in particle size, shape and crystallinity for time periods of at least eight months. It is therefore possible to keep ACC intact and make the suspensions needed for the treatment of calcareous stones.

### 3.2. Suspensions of Amorphous $\text{SiO}_2$ Particles

The particle size distribution of the  $\text{AmSiO}_2$  preparations described in the experimental section was monitored as a function of time. The stability of the  $\text{AmSiO}_2$  suspensions treated by sonication for time periods up to 7 min was examined. The mean particle size of the  $\text{AmSiO}_2$  suspensions was stable, at about 150–200 nm for a period of one month. Ultrasonic treatment over short time periods did not show any changes. However, ultrasonic treatment of the suspensions for longer times (5 and 7 min) caused the agglomeration of the suspended particles, as shown in Figure 9, in which the mean size of the suspensions treated for different duration times is shown as a function of time.

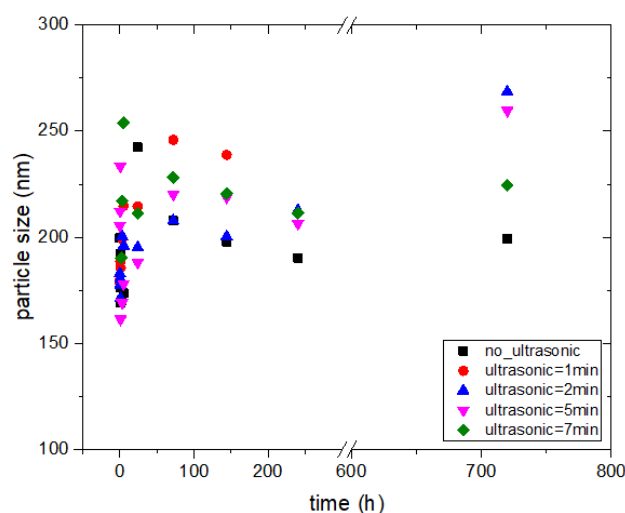


**Figure 9.** Mean particle diameter of  $\text{AmSiO}_2$  suspensions in the mother liquor, in the absence of CTAB as function of time, using ultrasonic treatment for 1, 2, 5, and 7 min.

The preparation obtained in the presence of low concentrations (1, 5 ppm) of CTAB consisted of particles with mean sizes of about 200 nm. In the presence of higher concentrations of CTAB (10 ppm), the mean particle size increased, as may be seen in Figure 10. It may be suggested that the apparent aggregation was due to the adsorption of the cationic surfactant adsorption on the negatively charged (in alkaline pH suspensions)  $\text{SiO}_2$  particles, which resulted in at least partial charge neutralization of their surface charge. As may be seen, the presence of 1 ppm CTAB did not have any significant effect, 5 ppm resulted in increases in the mean size by almost 50%, and the presence of 10 ppm CTAB yielded aggregated particles with a mean size of three times the respective size seen in the absence of CTAB. The concentration-dependent mean size increase is evidence of the respective surface charge neutralization.

The results of the XRD analysis (Figure 11) of the silica precipitates confirmed that the solids were amorphous to X-rays, both in the absence and in the presence of CTAB—which, as shown, did not affect the crystallinity of the precipitate. The entire XRD pattern did not show any reflection corresponding to crystalline materials, the total number of counts (intensity) of the diffracted X-rays was very low, and the pattern was typical for substances amorphous to X-rays. The morphology and particle size of the amorphous silica nanoparticles prepared by TEOS hydrolysis in the absence of CTAB are shown in the SEM pictures in Figure 12. The mean particle size was 100 nm and the preparation had a narrow size distribution. The larger mean particle size and the rather broad particle

size distribution of the preparations in the mother liquor apparently correspond to the formation of agglomerates which are stable over long time periods.

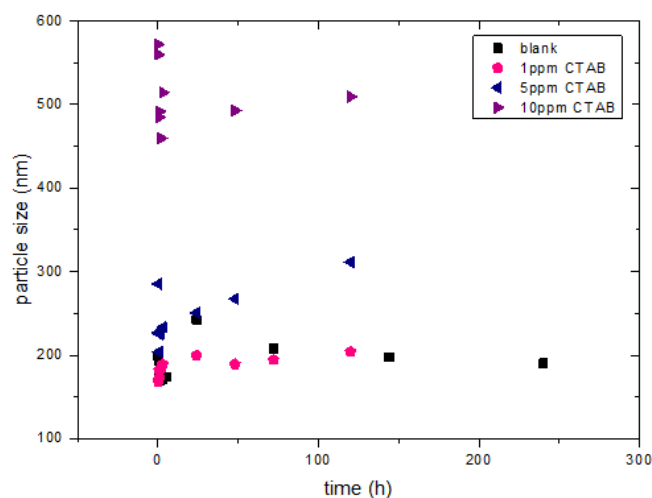


**Figure 10.** Mean particle diameter of AmSiO<sub>2</sub> particles suspended in water, as a function of time in the presence of the cationic surfactant CTAB.

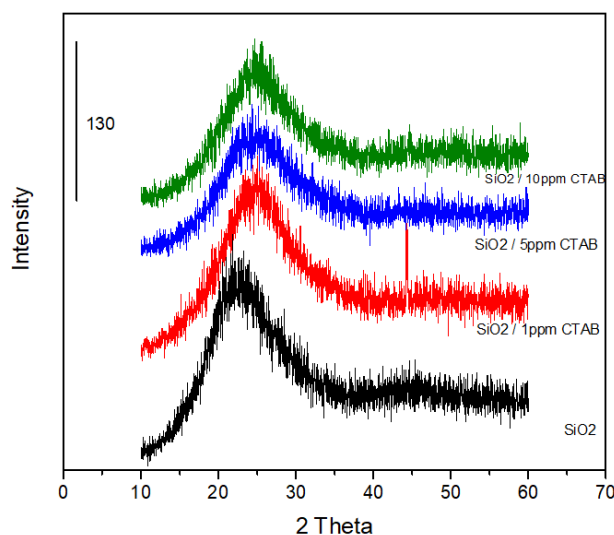


**Figure 11.** Powder X-ray diffraction pattern of SiO<sub>2</sub> particles precipitated by TEOS hydrolysis in the absence and in the presence of CTAB.

The results of the thermogravimetric analysis (TGA) for the AmSiO<sub>2</sub> nanoparticles prepared both in the absence and in the presence of CTAB are shown in Figure 13. The weight loss in the range of 100 to 300 °C observed was due to the residual organic part of TEOS (TEOH) after hydrolysis. No difference between solids prepared in the absence and in the presence of CTAB was observed.

### 3.3. Deposition of Nanoparticles in Pentelic Marble and Dissolution of Specimens (without and with Treatment with Suspensions)

The dissolution process takes place on the surface of the test specimens. In the present work, based on earlier work and in agreement with literature reports, it was assumed that at pH 6.50 dissolution is mainly controlled by surface diffusion of the crystal building units (possibly different from the crystal unit cell) on the surface of the crystals. The characteristic properties of the specimen surfaces are therefore very important for the kinetics of dissolution. In Table 2, the specific surface area and pore volume of powdered

Pentelic marble and of the materials, resulting from the deposition of ACC and AmSiO<sub>2</sub> nanoparticles, are summarized.

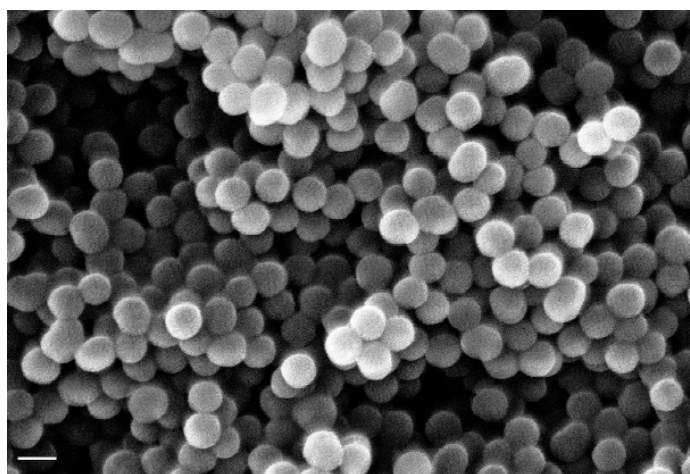


**Figure 12.** SEM picture of AmSiO<sub>2</sub> nanoparticles prepared by the hydrolysis of TEOS in the absence of CTAB (Bar 100 nm).

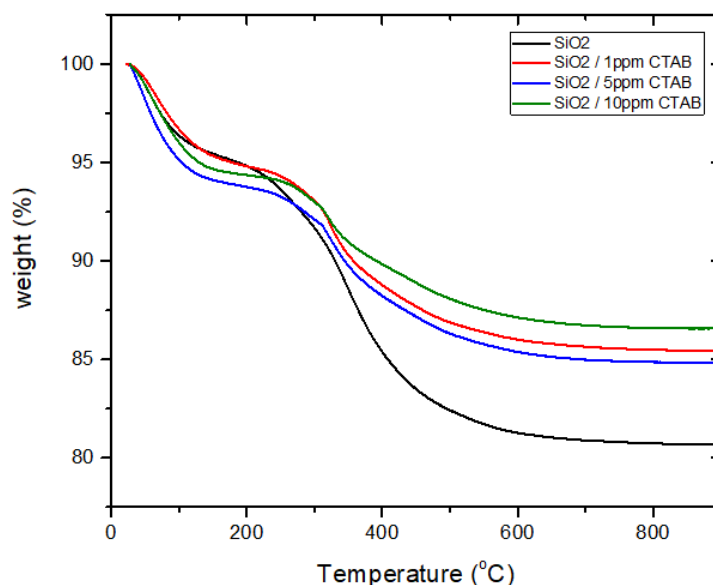


**Figure 13.** Thermogravimetric analysis (TGA) of AmSiO<sub>2</sub> nanoparticles prepared by TEOS hydrolysis in the absence and in the presence of the cationic surfactant CTAB.

As shown in Table 2, treatment of the PM surface with ACC nanoparticles reduced the specific surface area (SSA) and pore volume. This reduction suggested strong interactions between ACC and marble particles, which resulted in sealing of the larger pores. As may be seen, ACC particles adhering on marble irrespective of the method of application was ca. 3% *w/w*. Coating of PM grains with ACC nanoparticles is shown in the SEM pictures in Figure 14a,b, in which a rather thick layer of ACC has been formed. SiO<sub>2</sub> nanoparticles interacted to a larger extent with PM grains in suspension, as may be seen from the mass of silica retained on PM grains (ca. 14% *w/w*). The SSA of the solid increased to an extent that confirmed that the PM grain–AmSiO<sub>2</sub> composite was not just a mechanical mixture (a mechanical mixture of two components would be expected to yield an SSA ca. 11 m<sup>2</sup>·g<sup>−1</sup>). The concomitant increase of the pore volume of the composite material suggested that the deposition of the amorphous silica particles was done in “fluffy” layers, allowing for larger pores in the composite materials. In this sense, the deposition method AmSiB corresponded



to a more compact deposition, even though the weight percent deposit was the same as with AmSiA.

**Table 2.** Specific surface area (BET), pore volume (calculated from the BET isotherm) and amount of solid deposited on the powdered Pentelic marble.

Material	BET Specific Surface Area (m <sup>2</sup> /g)	Pore Volume (cm <sup>3</sup> /g)	% <i>w/w</i> CaCO <sub>3</sub> /SiO <sub>2</sub> in Material
Powdered Pentelic marble	8.4	0.029	
CaCO <sub>3</sub> (ACC)	4.7	0.006	
CCA method of CaCO <sub>3</sub> deposition	7.8	0.012	2.9
CCB method of CaCO <sub>3</sub> deposition	7.9	0.015	2.8
AmSiO <sub>2</sub>	32.5	0.103	
AmSiA method of SiO <sub>2</sub> deposition	23.7	0.110	13.9
AmSiB method of SiO <sub>2</sub> deposition	22.0	0.065	13.7

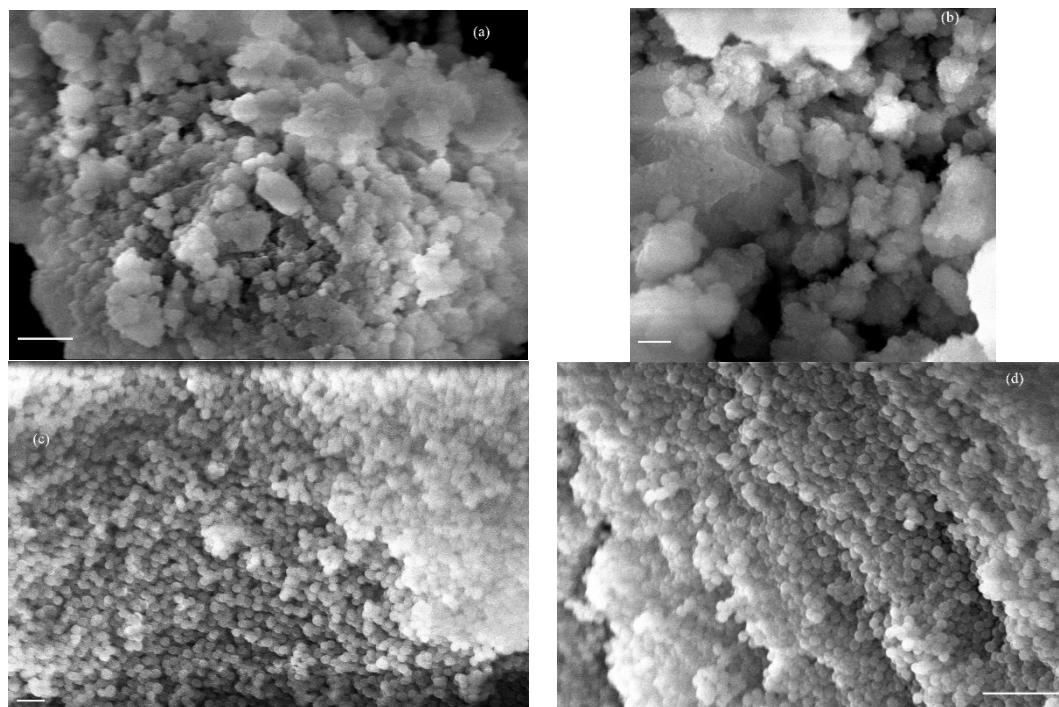


**Figure 14.** Surface coverage of PM grains by ACC: (a) ACC deposition, method CCA (bar 1  $\mu\text{m}$ ); (b) ACC deposition, method CCB (bar 200 nm); (c) Amorphous SiO<sub>2</sub> deposition method AmSiA (bar 200 nm); (d) Amorphous SiO<sub>2</sub> deposition method AmSiB (bar 1  $\mu\text{m}$ ).

The morphology of the PM grains covered by ACC and AmSiO<sub>2</sub> particles is shown in the SEM images of Figure 14.

The dissolution rates of all materials (PM grains, PM with ACC (methods CCA and CCB) and PM with SiO<sub>2</sub> (methods AmSiA and AmSiB)) were measured in solutions undersaturated with respect to calcite (thermodynamically the most stable calcium carbonate phase, which is the main chemical component of PM). The relative undersaturation,  $\sigma$ , of the solutions is defined as:

$$\sigma = 1 - \Omega^{\frac{1}{2}} \quad (2)$$



where

$$\Omega = \frac{(\text{Ca}^{2+})(\text{CO}_3^{2-})}{K_s^0} \quad (3)$$

In Equation (3), in the numerator is the product of the respective activities of the ions in the solution and  $K_s^0$  is the thermodynamic solubility constant for calcite. The maximum value of  $\Omega$  is 1 (saturated solution), where  $\sigma = 0$ . The experimental conditions for dissolution are summarized in Table 3:

**Table 3.** Composition and dissolution rates of marble using  $\text{CaCO}_3/\text{SiO}_2$  nanoparticles.

Material	Relative Undersaturation, $\sigma$	Dissolution Rate of $\text{CaCO}_3$ $/\times 10^{-8} \text{ mol}\cdot\text{m}^{-2}\cdot\text{s}^{-1}$
Powdered PM	0.89	1.4
$\text{CaCO}_3$ (ACC)		3.4
CCA		1.3
CCB		2.0
$\text{AmSiO}_2$		N/A
AmSiA		0.3
AmSiB		0.4

The dissolution rate of the PM with ACC deposited with both methods yielded rates of dissolution close to those corresponding to PM. The ACC coating is expected to dissolve faster in comparison to PM because of its higher solubility (Figure 15).

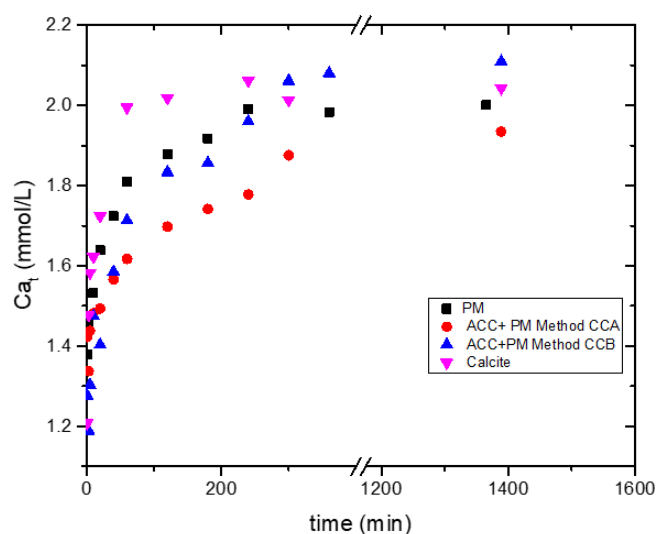


**Figure 15.** Dissolution of PM in undersaturated calcium carbonate solutions ( $\sigma = 0.89$ ), 25 °C, pH 6.50, 0.15 M NaCl; (■) PM untreated; (●) PM with ACC deposits, method CCA; (▲) PM with ACC deposits, method CCB; (▼) calcite powder.

As may be seen in Figure 15, the rates and the overall dissolution of PM was reduced with treatments of deposition of ACC with methods CCA and CCB. The former method, in which precipitation of ACC was induced in the solution in the presence of DMC was more efficient, apparently due to stronger interactions with the PM grains. It is interesting that the application of ACC on the PM, irrespective of the method of application, reduced the rate of dissolution, despite the fact that ACC is more soluble than the calcite—as may be also seen from the dissolutions kinetics of the model compound (calcite).

Amorphous silica deposits on PM grains by the two methods (AmSiA and AmSiB), resulted in the slowing of the dissolution of PM, as may be seen in Figure 16.

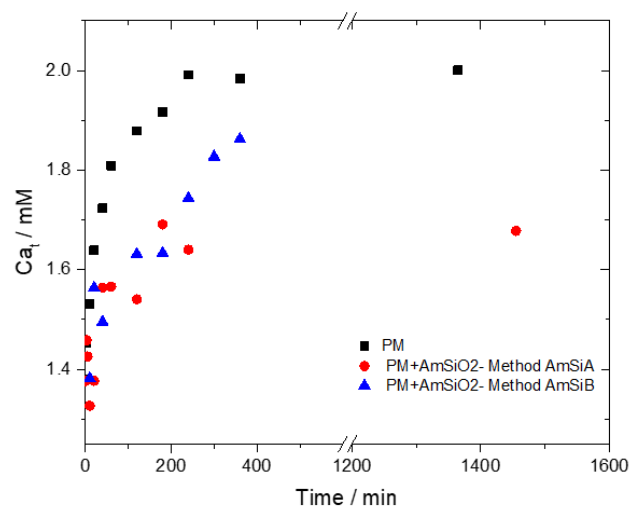


**Figure 16.** Dissolution of PM in undersaturated calcium carbonate solutions ( $\sigma = 0.89$ ), 25 °C, pH 6.50, 0.15 M NaCl; (■) PM untreated; (●) PM with AmSiO<sub>2</sub> deposits, method AmSiA; (▲) PM with AmSiO<sub>2</sub> deposits, method AmSiB.

The deposits of amorphous silica were quite efficient in reducing the rates of dissolution of PM in acidic aqueous media, especially when applied in the same way as ACC, i.e., when the coating is applied by precipitation in a suspension of the underlying material (method AmSiA).

#### 4. Conclusions

Suspensions of ACC were successfully synthesized by the hydrolysis of DMC in the presence of calcium chloride solutions at very alkaline conditions. The stability of the suspensions in the mother liquor depends on the composition of the solutions from which it precipitates out. Stable ACC suspensions were obtained from solutions in which DMC concentration was 50mM, CaCl<sub>2</sub> 10 mM and NaOH 100 mM. Higher concentrations yielded precipitates in which vaterite and portlandite dominated the solid phase. The ACC obtained by separation from the mother liquor was quite stable in the solid form at −24 °C, and suspensions in isopropanol were stable at least for 9 days. In the presence of 1, 10 and 100 ppm of the cationic surfactant CTAB, the stability of the suspensions was not favored and the less stable vaterite was converted into calcite. ACC suspensions were applied successfully on finely comminuted PM.

Amorphous silica suspensions were prepared by TEOS hydrolysis. These suspensions consisted of fairly monodispersed silica particles with sizes of 100 nm. The mean particle size measured by laser diffraction was larger, suggesting aggregation. The formation of aggregates was intensified in the presence of the cationic surfactant CTAB.

The most effective method of application of ACC and AmSiO<sub>2</sub> on PM was found to be the formation of the two types of nanoparticles in suspensions of PM grains. This process is equivalent to brushing or spraying surfaces with the suspensions. The deposition of both ACC and AmSiO<sub>2</sub> on PM resulted in a significant reduction of the respective rates of dissolution in solutions undersaturated with respect to calcium carbonate at pH 6.50.

**Author Contributions:** Conceptualization, P.G.K., C.A.P., E.I.P.; methodology, E.I.P., P.G.K.; validation, T.G.T., C.L., E.Z.; formal analysis, E.I.P., T.G.T., C.L., E.Z.; investigation, E.I.P., T.G.T., C.L., E.Z.; resources, P.G.K., C.A.P.; data curation, A.G.A., T.G.T.; writing—original draft preparation, E.I.P., P.G.K., C.A.P.; visualization, E.I.P., P.G.K., C.A.P.; supervision, P.G.K., C.A.P.; project administration, P.G.K., C.A.P.; funding acquisition, P.G.K. All authors have read and agreed to the published version of the manuscript.

**Funding:** This research was funded by Western Greece Region, ESPA Programme of Regional Development, Program KRHPIS II, Action POLITEIA II, grant number MIS 5002478.

**Institutional Review Board Statement:** Not applicable.

**Informed Consent Statement:** Not applicable.

**Data Availability Statement:** The Study did not include report data included in publicly open databases.

**Acknowledgments:** Part of this work was carried out as part of the research project «Ανάπτυξη νέων υλικών για τη συντήρηση διαβρωμένων ασβεστολιθικών δομικών στοιχείων» στο πλαίσιο της πράξης με τίτλο «Πολιτισμός Τεχνολογία: Νέες Τεχνολογίες στην Έρευνα, Μελέτη, Τεκμηρίωση και Πρόσβαση στην Πληροφορία Αντικειμένων Πολιτισμικής Κληρονομιάς και Μνημείων (ΠΙΟΛΙΤΕΙΑ-II)» με Κωδικό ΟΠΣ 5002478; Part of this work was financially supported by the Stavros Niarchos Foundation within the framework of the project ARCHERS; Laboratory of Instrumental Pharmaceutical Analysis, Department of Pharmacy, University of Patras, is acknowledged for the micro Raman spectroscopy characterizations.

**Conflicts of Interest:** The authors declare no conflict of interest.

## References

1. Spathis, P.; Triantafyllidis, K.; Prochaska, C.; Karapanagiotis, I.; Pavlidou, E.; Stefanidou, M. Characterization and properties of silicate and nanocomposite coatings for the protection of dolomite marble against weathering. In *International Symposium on the Conservation of Monuments in the Mediterranean Basin*; Springer: Cham, Switzerland, 2018; pp. 287–294. [\[CrossRef\]](#)
2. Baglioni, P.; Chelazzi, D.; Giorgi, R.; Poggi, G. Colloid and materials science for the conservation of cultural heritage: Cleaning, consolidation, and deacidification. *Langmuir* **2013**, *29*, 5110–5122. [\[CrossRef\]](#)
3. Sadat-Shojai, M.; Ershad-Langroudi, A. Polymeric coatings for protection of historic monuments: Opportunities and challenges. *J. Appl. Polym. Sci.* **2009**, *112*, 2535–2551. [\[CrossRef\]](#)
4. Baglioni, P.; Carretti, E.; Chelazzi, D. Nanomaterials in art conservation. *Nat. Nanotechnol.* **2015**, *10*, 287–290. [\[CrossRef\]](#)
5. De Ferri, L.; Lottici, P.P.; Lorenzi, A.; Montenero, A.; Salvioli-Mariani, E. Study of silica nanoparticles—Polysiloxane hydrophobic treatments for stone-based monument protection. *J. C. Herit.* **2011**, *12*, 356–363. [\[CrossRef\]](#)
6. Ksinopoulou, E.; Bakolas, A.; Moropoulou, A. Modification of Si-based consolidants by the addition of colloidal nanoparticles: Application in porous stones. *J. Nano Res.* **2014**, *27*, 143–152. [\[CrossRef\]](#)
7. Kapridaki, C.; Maravelaki-Kalaitzaki, P. TiO<sub>2</sub>-SiO<sub>2</sub>-PDMS nano-composite hydrophobic coating with self-cleaning properties for marble protection. *Prog. Org. Coat.* **2013**, *76*, 400–410. [\[CrossRef\]](#)
8. Kapridaki, C.; Maravelaki-Kalaitzaki, P. TiO<sub>2</sub>-SiO<sub>2</sub>-PDMS nanocomposites with self-cleaning properties for stone protection and consolidation. *Geol. Soc. Lond. Spec. Publ.* **2015**, *416*, 285–292. [\[CrossRef\]](#)
9. Manoudis, P.; Papadopoulou, S.; Karapanagiotis, I.; Tsakalof, A.; Zuburtikudis, I.; Panayiotou, C. Polymer-silica nanoparticles composite films as protective coatings for stone-based monuments. *J. Phys. Conf. Ser.* **2007**, *61*, 1361–1365. [\[CrossRef\]](#)
10. Aldoasri, M.A.; Darwish, S.; Adam, M.; Elmarzugi, N.; Ahmed, S. Performance of Clay, SiO<sub>2</sub>, Ca(OH)<sub>2</sub> and CaCO<sub>3</sub>-polymeric nanocomposites for conservation and preservation of limestone artworks. *Preprints* **2018**. [\[CrossRef\]](#)
11. Aldoasri, M.A.; Darwish, S.S.; Adam, M.A.; Elmarzugi, N.A.; Ahmed, S.M. Enhancing the durability of calcareous stone monuments of Ancient Egypt using CaCO<sub>3</sub> nanoparticles. *Sustainability* **2017**, *9*, 1392. [\[CrossRef\]](#)
12. Burgos-Cara, A.; Rodríguez-Navarro, C.; Ortega-Huertas, M.; Ruiz-Agudo, E. Bioinspired alkoxysilane conservation treatments for building materials based on amorphous calcium carbonate and oxalate nanoparticles. *ACS Appl. Nano Mater.* **2019**, *2*, 4954–4967. [\[CrossRef\]](#)
13. Manoudis, P.N.; Karapanagiotis, I.; Tsakalof, A.; Zuburtikudis, I.; Kolinkeová, B.; Panayiotou, C. Superhydrophobic films for the protection of outdoor cultural heritage assets. *Appl. Phys. A* **2009**, *97*, 351–360. [\[CrossRef\]](#)
14. Giorgi, R.; Ambrosi, M.; Toccafondi, N.; Baglioni, P. Nanoparticles for cultural heritage conservation: Calcium and bariumhydroxide nanoparticles for wall painting consolidation. *Chem. Eur. J.* **2010**, *16*, 9374–9382. [\[CrossRef\]](#) [\[PubMed\]](#)
15. Baglioni, M.; Poggi, G.; Chelazzi, D.; Baglioni, P. Advanced materials in cultural heritage conservation. *Molecules* **2021**, *26*, 3967. [\[CrossRef\]](#) [\[PubMed\]](#)
16. Rodríguez-Navarro, C.; Ruiz-Agudo, E. Nanolimes: From synthesis to application. *Pure Appl. Chem.* **2018**, *90*, 523–550. [\[CrossRef\]](#)
17. Dei, L.; Salvadori, B. Nanotechnology in cultural heritage conservation: Nanometric slaked lime saves architectonic and artistic surfaces from decay. *J. C. Herit.* **2006**, *7*, 110–115. [\[CrossRef\]](#)
18. Rodríguez-Navarro, C.; Kudłacz, K.; Cizer, O.; Ruiz-Agudo, E. Formation of amorphous calcium carbonate and its transformation into mesostructured calcite. *CrystEngComm* **2015**, *17*, 58–72. [\[CrossRef\]](#)
19. Sierra-Fernandez, A.; Gomez-Villalba, L.S.; Rabanal, M.E.; Fort, R. New nanomaterials for applications in conservation and restoration of stony materials: A review. *Mater. Constr.* **2017**, *67*, 3–17. [\[CrossRef\]](#)
20. Kanellopoulou, D.G. Physico-Chemical Investigation of the Deterioration of Building Materials of Historic Monuments and Protection Methods. Ph.D. Thesis, University of Patras, Patra, Greece, 2012; p. 151.
21. Koga, N.; Nakagoe, Y.; Tanaka, H. Crystallization of amorphous calcium carbonate. *Thermochim. Acta* **1998**, *318*, 239–244. [\[CrossRef\]](#)

22. Faatz, M.; Gröhn, F.; Wegner, G. Amorphous calcium carbonate: Synthesis and potential intermediate in biomineralization. *Adv. Mater.* **2004**, *16*, 996–1000. [[CrossRef](#)]
23. Singh, T.K.; Jain, C.L.; Sharma, S.K.; Singh, S.S. Preparation of dispersed silica by hydrolysis of tetraethyl orthosilicate. *Indian J. Eng. Mater. Sci.* **1999**, *6*, 349–351.
24. Vagenas, N.V.; Gatsouli, A.; Kontoyannis, C.G. Quantitative analysis of synthetic calcium carbonate polymorphs using FT-IR spectroscopy. *Talanta* **2003**, *59*, 831–836. [[CrossRef](#)]
25. Khouzani, M.F.; Chevrier, D.M.; Güttlein, P.; Hauser, K.; Zhang, P.; Hedinc, N.; Gebauer, D. Disordered amorphous calcium carbonate from direct precipitation. *CrystEngComm* **2015**, *17*, 4842–4849. [[CrossRef](#)]
26. Chakrabarty, D.; Mahapatra, S. Aragonite crystals with unconventional morphologies. *J. Mater. Chem.* **1999**, *9*, 2953–2957. [[CrossRef](#)]
27. Xyla, A.G.; Koutsoukos, P.G. Quantitative analysis of calcium carbonate polymorphs by infrared spectroscopy. *J. Chem. Soc. Faraday Trans. 1 Phys. Chem. Condens. Phases* **1989**, *85*, 3165–3172. [[CrossRef](#)]
28. Rodriguez-Blanco, J.D.; Shaw, S.; Benning, L.G. The kinetics and mechanisms of amorphous calcium carbonate (ACC) crystallization to calcite, viavaterite. *Nanoscale* **2011**, *3*, 265–271. [[CrossRef](#)] [[PubMed](#)]
29. Siva, T.; Muralidharan, S.; Sathiyarayanan, S.; Manikandan, E.; Jayachandran, M. Enhanced polymer induced precipitation of polymorphous in calcium carbonate: Calcite aragonite vaterite phases. *J. Inorg. Organomet. Polym. Mater.* **2017**, *27*, 770–778. [[CrossRef](#)]
30. Khachani, M.; El Hamidi, A.; Halim, M.; Aarsalane, S. Non-isothermal kinetic and thermodynamic studies of the dehydroxylation process of synthetic calcium hydroxide  $\text{Ca}(\text{OH})_2$ . *J. Mater. Environ. Sci.* **2014**, *5*, 615–624.
31. Nehrke, G.; Poigner, H.; Wilhelms-Dick, D.; Brey, T.; Abele, D. Coexistence of three calcium carbonate polymorphs in the shell of the Antarctic clam *Laternula elliptica*. *Geochem. Geophys. Geosyst.* **2012**, *13*, 1–8. [[CrossRef](#)]
32. Behrens, G.; Kuhn, L.T.; Ubig, R.; Heuer, A.H. Raman spectra of vateritic calcium carbonate. *Spectrosc. Lett.* **1995**, *28*, 983–995. [[CrossRef](#)]
33. Rodriguez-Navarro, C.; Elert, K.; Ševčík, R. Amorphous and crystalline calcium carbonate phases during carbonation of nanolimes: Implications in heritage conservation. *CrystEngComm* **2016**, *18*, 6594–6607. [[CrossRef](#)]